Zebrafish modeling mimics developmental phenotype of patients with RAPGEF1 mutation

Na Li[1], Pei Zhou[1], Miaomiao Yang[1], Xiang Fang[1], Nadine Krämer[2], Tauqeer Ahmed Mughal[3], Ansar Abbassi[4], Angela Kaindl[2], and Hao Hu[1]

[1]Guangzhou Women and Children's Medical Center
[2]Charité Universitätsmedizin Berlin
[3]Mirpur University of Science and Technology
[4]Department of Zoology

December 1, 2020

Abstract

RAPGEF1 is a guanine nucleotide exchange factor responsible for transmitting extracellular signals to the Ras family of GTPase located at the inside of membrane. Here, we report for the first time a homozygous mutation of RAPGEF1 in a consanguineous family with two siblings affected by neuropsychiatric disorder. To confirm the correlation of the mutation and the phenotype, we utilized in silico analysis and established a zebrafish model. Survival rate was reduced in the rapgef1a-knockdown model, and the zebrafish showed global morphological abnormalities, particularly of brain and blood vessels. Co-application of human RAPGEF1 wildtype mRNA effectively rescued the abnormal phenotype, while that of RAPGEF1 mRNA carrying the human mutation did not. This work is the first report of a human Mendelian disease associated with RAPGEF1 and the first report of a zebrafish model built for this gene. The phenotype of zebrafish model provides further evidence that defective RAPGEF1 may lead to global developmental delay in human patients.

Introduction:

Cells receive molecular cues from the extracellular matrix through receptors located at the cell membrane to regulate pivotal functions such as cell proliferation, migration, and differentiation. The signals from outside of cells are transmitted through adaptor proteins and guanine nucleotide exchange factors to small GTPases, which activate the downstream targets subsequently. Maintenance of these signaling pathways is of critical importance in cell survival and organism development. On the contrary, their perturbation can cause aberrant cell properties and abnormal tissue development. RAPGEF1 is a guanine nucleotide exchange factor transmitting signals from the extracellular matrix to the Ras family of GTPase, by modulating the Ras/Rap/MAPK pathway and Ras/Jun kinase pathway (Voss, Gruss, & Thomas, 2003; Voss, Krebs, & Thomas, 2006). RAPGEF1 was found to be present in a complex with CRK or GRB2/ASH, transducing signals from tyrosine kinases to RAS in a number of different tissues (Tanaka et al., 1994). The RAS-CRK-RAP1 cellular signal transduction system is regulated by guanine nucleotide exchange factors (GEFs), derangement of which could lead to carcinogenesis (Hirata et al., 2004).

Rapgef1 is essential for embryonic development, and *Rapgef1* null mouse embryos died early in gestation (Ohba et al., 2001). Mice embryos with hypomorphic alleles of *Rapgef1* could sustain longer, but still died due to blood vessel maturation defects (Voss et al., 2003). Rapgef1 is required for the formation of focal adhesion and vascular maturation, accounting for blood vessel development defect in mouse models (Voss et al., 2003). Rapgef1 has also been shown to regulate pathological angiogenesis in tumors by mediating platelet secretion (Martin-Granado et al., 2017). Further evidence exists for a role of Rapgef1 in myogenic

differentiation through coordination cell cycle exit, actin dynamics and survival signaling (Sasi Kumar et al., 2015) and in the regulation of the cortical neural precursor population size through Rapgef1-mediated inhibition of the Ras signaling pathway (Voss et al., 2006). Mice lacking Rapgef1 had an increase in nuclear beta-catenin and a prominent increase of neural precursor proliferation in the cerebral cortex (Voss et al., 2006). Rapgef1-deficient mouse embryos also showed a failure of cortical neurons to migrate (Voss et al., 2008). Rapgef1 was shown to be involved in the multi-to-bipolar transition in mouse cortex during neuronal development, defects of which caused failure in neuronal migration, axon formation and cortical lamination (Shah et al., 2016).

There is no report of human Mendelian disease attributable to*RAPGEF1* . We noted that, a relevant gene, namely, *RAPGEF2*(OMIM#609530), was supposed to be related to familial myoclonic epilepsy. Given the phenotype observed in the aforementioned*Rapgef1* mouse models, it is reasonable to hypothesize that the hypomorphic alleles of *RAPGEF1* may cause problems in multiple systems especially brain and vessel. Zebrafish is a widely used organismal model for mimicry of human developmental disorders. Recapitulating human phenotype by zebrafish models can provide insights into the molecular mechanism of *RAPGEF1* defects.

Materials and methods:

Pedigree recruitment and genetic screening

The participating family of Pakistani descent was recruited from the Jammu and Kashmir for this study. The study was approved by the institutional ethical review boards of Mirpur University of Science and technology (MUST) and by the ethic committee of the Charité (EA1/212/08). Written informed consents were obtained from all individuals or custodians for the participation in the study. The behavior and phenotype of all affected individuals was analyzed with special attention to neurological, morphological, ophthalmological, dermatological and skeletal symptoms.

Genomic DNA from one affected and one not affected family member was extracted from the peripheral blood by using the QIAamp DNA blood mini kit (Qiagen, Frankfurt, Germany) according to the manufacturer's instructions. The whole exome sequencing procedures were performed on a HiSeq4000 deep sequencer (Illumina, CA, USA) with a 150 bp paired-end protocol after enrichment in the coding regions by the SureSelect Human All Exon V5 kits (Agilent, CA, USA). The average sequencing coverage reached more than 150X, with at least 20X of more than 99% of the coding regions. The generated raw sequences were processed by the MERAP package for alignment, quality control, calling single nucleotide variant (SNV), insertion and deletion (Indel), structural variation (SV), and copy number variation (CNV), plus the variants annotation and prioritization (Hu et al., 2014). PCR amplification was performed by using the Q5 High-Fidelity Polymerase (5X, NEB, MA, USA) with the following specific primers targeted to the selected candidate variant: Forward: 5'-GTTTCCAGTGCCACCAAACC-3', Reverse: 5'-AGCAAGAGCCTTTCCATTCCT-3'. The PCR products were Sanger sequenced to determine the carrier status of the specific variant.

Bioinformatics analysis procedure

We filtered all identified variants through comparison with the disease-associated variants in the Human Gene Mutation Database (HGMD, 2020.2) and the Online Mendelian Inheritance in Man (www.omim.org), dbSNP153 (http://www.ncbi.nlm.nih.gov/projects/SNP/), the 1000 Genome (http://www.1000genomes.org/), the NHLBI Exome Sequencing Project (ESP, http://evs.gs.washington.edu/EVS/), and GnomAD (https://gnomad.broadinstitute.org/). To assess the pathogenicity of missense mutations, we generated the prediction of a variety of algorithms, including SIFT (https://sift.bii.a-star.edu.sg/), PolyPhen2 (http://genetics.bwh.harvard.edu/pph2/), and Mutation-Taster (http://www.mutationtaster.org/). The pathogenic and likely pathogenic genes/variants were defined according to the standards and guidelines of ACMG (Richards et al., 2015).

Domains of RAPGEF1 were identified by the SMART protein domain prediction server (http://smart.embl-heidelberg.de/). Multiple sequence alignments of RAPGEF1 were performed using the ClustalW program

(Thompson, Gibson, & Higgins, 2002). Three-dimensional structural models of RAPGEF1 were predicted by the I-TASSER web tool (http://zhang.bioinformatics.ku.edu/I-TASSER/). The visual representation of models and structural superposition were generated by the software package of visual molecular dynamics (VMD) (Humphrey, Dalke, & Schulten, 1996). The mutant stability change ($\Delta\Delta$G) of variants of RAPGEF1 were predicted using the STRUM server (https://zhanglab.ccmb.med.umich.edu/STRUM/). KEGG pathway analysis was performed on *RAPGEF1* and ˜700 genes known to be related to neurodevelopmental disorders (Vissers, Gilissen, & Veltman, 2016) using pathway enrichment analysis tool of Omicshare (https://www.omicshare.com/tools/home/report/koenrich.html). Three pathways involving *RAPGEF1* were selected. Protein-protein interaction data between RAPGEF1 and neurodevelopmental disorder-related proteins were obtained from the STRING database (https://string-db.org/). The interaction network model was generated with the package of Cytoscape (Shannon et al., 2003).

Zebrafish Care and Maintenance

Adult wild-type AB strain zebrafish were maintained at 28.5 on a 14 h light/10 h dark cycle (Westerfield, 2000). Five to six pairs of zebrafish were set up for nature mating every time. On average, 200–300 embryos were generated. Embryos were maintained at 28.5 in fish water (0.2% Instant Ocean Salt in deionized water). The embryos were washed and staged according to (Kimmel, Ballard, Kimmel, Ullmann, & Schilling, 1995). The establishment and characterization of *hb9-EGFP* and*fli1a-EGFP* transgenic lines has been described elsewhere (Kanungo, Lantz, & Paule, 2011; Lawson & Weinstein, 2002). The zebrafish facility is accredited by the Association for Assessment and Accreditation of Laboratory Animal Care (AAALAC) International.

Zebrafish microinjections

Gene Tools, LLC (http://www.gene-tools.com/) designed the morpholino (MO). Antisense MOs (GeneTools) were microinjected into fertilized one-cell stage embryos according to standard protocols (Nasevicius & Ekker, 2000). The sequences of the *rapgef1a* translation-blocking and splice-blocking morpholinos were 5'-TGTCTATTTTCCCAGACATCTTGCT-3' (ATG-MO) and 5'-GACGCTTAAAAACATTTTACCTGCT-3' (E2I2-MO), respectively. The sequence for the standard control morpholino was 5'-CCTCTTACCTCAGTTACAATTTATA-3' (Gene Tools). The amount of the MOs used for injection was as follows: Control-MO and E2I2-MO, 1 ng per embryo; ATG-MO, 2ng per embryo. Total RNA was extracted from 30 to 50 embryos per group in TriPure Isolation Reagent (Roche) according to the manufacturer's instructions. RNA was reverse transcribed using the PrimeScript RT reagent Kit with gDNA Eraser (Takara). Primers spanning*rapgef1a* exon 1 (forward primer: 5‘-CCACCAGAACAACCCGTAAA-3') and exon 3 (reverse primer: 5‘-ATTCACACCCTCCAGCATTAC-3') were used for RT-PCR analysis for confirmation of the efficacy of the E2I2-MO. The primer ef1α sequences used as the internal control were 5‘-GGAAATTCGAGACCAGCAAATAC-3' (forward) and 5‘-GATACCAGCCTCAAACTCACC-3' (reverse). For rescue experiments, 2ng rapgef1a-E2I2-MO was co-injected with 50 pg pcDNA3.1 containing human *RAPGEF1* (nonmutant and mutant) cDNA per embryo respectively. The coding region of the wild-type or mutant human *RAPGEF1* was synthesized by Sangon Biotech and subcloned into pcDNA3.1 vector (Invitrogen).

Zebrafish spinal motor neurons studies

To evaluate spinal motor neurons formation in zebrafish, fertilized one-cell hb9-EGFP transgenic lines embryos were injected with control-MO and rapgef1a-MO. At 36-hpf, embryos were dechorionated, anesthetized with 0.016% MS-222 (tricaine methanesulfonate, Sigma-Aldrich, St. Louis, MO). Zebrafish were then oriented on their lateral side (anterior, left; posterior, right; dorsal, top) or dorsal side, and mounted with 3% methylcellulose in a depression slide for observation by fluorescence microscopy. The morphological parameters of spinal motor neurons were quantitatively analyzed (Kanungo et al., 2011; Nakano, Windrem, Zappavigna, & Goldman, 2005; Paquet et al., 2009).

Zebrafish angiogenesis studies

To evaluate blood vessel formation in zebrafish, fertilized one-cell fli1a-EGFP transgenic lines embryos were

injected with rapgef1a-MO and control-MO. At 48-hpf, embryos were dechorionated, anesthetized with 0.016% MS-222 (tricaine methanesulfonate, Sigma-Aldrich, St. Louis, MO). Zebrafish were then oriented on lateral side (anterior, left; posterior, right; dorsal, top), and mounted with 3% methylcellulose in a depression slide for observation by fluorescence microscopy. The phenotypes of complete intersegmental vessels (ISVs) (i.e. the number of ISVs that connect the DA to the DLAV) were quantitatively analyzed. The characterization of vasculature system and its development was described previously (Benedito et al., 2012; Covassin, Villefranc, Kacergis, Weinstein, & Lawson, 2006; Noguera-Troise et al., 2006; Ridgway et al., 2006; Siekmann & Lawson, 2007; Wythe et al., 2013).

Behavioral analysis

Experiments were carried out at 5-dpf. At 5-dpf, the larvae were collected, cleaned and placed in 96-well plates. Each well contained 0.2 mL of fish water and one larva. Behavioral tests were performed as following: the larvae were allowed to acclimate for 15 min before locomotion monitoring (Zhao et al., 2012). Next, the larvae were allowed to freely explore the aquarium for 30 minutes. A camera positioned above the plate was used for movement tracking. All digital tracks were analyzed by Ethovision XT software (Noldus Information Technology, Wageningen, Netherlands), and system noise was filtered out with a minimum movement distance of 0.2 mm. Four parameters, including the total movement distance, velocity, mobility and maximum acceleration were analyzed.

Image acquisition and statistical analysis

Embryos and larvae were analyzed with Nikon SMZ 18 Fluorescence microscope and subsequently photographed with digital cameras. A subset of images was adjusted for levels, brightness, contrast, hue and saturation with Adobe Photoshop 7.0 software (Adobe, San Jose, California) to optimally visualize the expression patterns. Quantitative image analyses processed using image based morphometric analysis (NIS-Elements D4.6, Japan) and ImageJ software (U.S. National Institutes of Health, Bethesda, MD, USA; http://rsbweb.nih.gov/ij/). Inverted fluorescent images were used for processing. Positive signals were defined by particle number using ImageJ. 10 animals for each treatment were quantified and the total signal per animal was averaged. All data are presented as mean ± SEM. Statistical analysis and graphical representation of the data were performed using GraphPad Prism 5.0 (GraphPad Software, San Diego, CA). Statistical significance was performed using a Student's t test , ANOVA, or $\chi 2$ test as appropriate. Statistical significance is indicated by *, where $P < 0.05$, and ***, where $P < 0.0001$.

Results:

Identification of homozygous *RAPGEF1* variant in patients with neuropsychiatric phenotype

The two siblings (IV.2 and IV.3) of a consanguineous family of Pakistani descent showed moderate intellectual disability, mood swings from a depressive to a jolly mood, repetitive behavior, visual impairment and no speech development in one individual (IV.3) (Figure 1 (A) and (C)). By using whole exome sequencing on one of the patients (IV.2) and the father (III.4), we detected the missense variant c.423G>A (NM_198679.1, NP_941372.1:p.(M141I)) in the *RAPGEF1* gene. Targeted PCR and subsequent Sanger sequencing confirmed that this variant was homozygous in the patient and heterozygous in the father, matching a presumed recessive inheritance mode (Figure 1 (B)).

RAPGEF1 encodes a RAP guanine nucleotide exchange factor (OMIM#600303). The expression of this gene starts early in mice embryos where it reaches its climax by E15.5 with enrichment in the murine forebrain (https://www.ebi.ac.uk/gxa/home). The variant identified in this gene has a very low frequency in the population databases, is predicted to be pathogenic by various algorithms (Figure 2 (A)) and to cause an alteration of a conserved amino acid, which is located in a protein domain (Figure 2 (B) and (C)). The structural modeling of RAPGEF1 indicates a dramatic decrease of protein stability, which we propose to account for a dysfunction in the patients (Figure 2 (D)). Interestingly, the protein-protein interaction network plus KEGG pathway analysis reveals three functional modules in which RAPGEF1 plays important roles (Figure 2 (E)).

Morpholino nucleotides specifically blocked the splicing or translation of *rapgef1* in zebrafish

RAPGEF1 is highly conserved through a multitude of species including zebrafish (*Danio rerio*). The homologous gene of human*RAPGEF1* in zebrafish is *rapgef1a* (ENSDART00000139947.3). To simulate the function of human *RAPGEF1* , we knocked down the expression of zebrafish *rapgef1a* by two morpholino nucleotides, targeting the proper splicing (E2I2-MO) and translation (ATG-MO) of*rapgef1a* , respectively (Figure 3 (A)). The effectiveness of the E2I2-MO was confirmed by testing the presence of skipped exon 2 in the transcripts of morpholino-injected embryos 3 days after fertilization (Figure 3 (B)).

rapgef1-**knockdown reduced survival rate and caused alteration in gross morphology**

Both E2I2-MO and ATG-MO exerted negative influences on the gross morphology of zebrafish. We observed general abnormality of*rapgef1a* -knockdown zebrafish embryos, especially in the curved body axis and brain patterns (Figure 4 (A) and (B)). The percentage of embryos with body defects was much higher in *rapgef1a* -knockdown animals than in controls (Figure 4 (C)). Also, the survival rate of zebrafish embryos for a 5-day time course was significantly lower in the*rapgef1a* -knockdown group than in controls (Figure 4 (C)).

To evaluate the deleterious effect of human mutant *RAPGEF1*transcript and as a proof-of-concept approach, we co-injected the E2I2-MO and the human *RAPGEF1* transcripts with and without the aforementioned patient mutation. The rescuing capacity of human wildtype*RAPGEF1* transcript was obvious in the zebrafish with curved body axis and brain patterning defects, while the human mutant *RAPGEF1*transcript showed no rescue effect (Figure 4 (D) and (E)). In parallel, the percentage of embryos with defects was to some extent promoted by the human wildtype *RAPGEF1* transcript but not by the mutant one (Figure 4 (F)). The same effect was observed in the survival rate (Figure 4 (F)).

rapgef1-**knockdown reduced locomotor capacity and led to irregular motor neuron axon**

Both E2I2-MO and ATG-MO exerted negative influences on the locomotor capacity and motor neuron axon of zebrafish. We observed obvious reduction in the movement parameters of *rapgef1a* -knockdown zebrafish larvae in the *rapgef1a* -knockdown group when compared to controls, including the moving velocity and distance (Figure 5 (A) and (B)). To evaluate the deleterious effect of human mutant *RAPGEF1*transcript, we again co-injected the E2I2-MO and human *RAPGEF1*transcripts with and without the aforementioned patient mutation. As expected from the previous proof-of-concept experiments, the rescuing capacity of human wildtype *RAPGEF1* transcript was much higher than that of the mutant one, with the movement parameters recovered to the normal degree (Figure 5 (C) and (D)).

We also observed apparently abnormal spinal motor neuron arborization in the *rapgef1a* -knockdown zebrafish larvae, either with E2I2-MO or ATG-MO. The motor neuron presented a lower number of axons with incomplete and ectopic sprouts (Figure 5 (E) and (G)). The co-injection of E2I2-MO and human wildtype *RAPGEF1* mRNA effectively rescued the phenotype but the co-injection with human mutant *RAPGEF1* mRNA failed to do so (Figure 5 (F) and (G)).

rapgef1-**knockdown induced vascular defects and abnormal somitogenesis**

Both the E2I2-MO and ATG-MO effectively knocked down the expression of*rapgef1a* and caused abnormal vessel structure and somitogenesis (Figure 6 (A) and (B)). By using *Tg(fli1a:EGFP)* zebrafish embryos, we observed irregular vascular microstructure including a lower number of incomplete ISV (intersegmental vessel) and ectopic sprouts (Figure 6 (A)). Meanwhile, *rapgef1a* -knockdown caused the gross somite morphology alteration, from a normal V-shape to an abnormal U-shape (Figure 6 (B)). As expected, the co-injection of E2I2-MO and human wildtype *RAPGEF1* mRNA rescued the abnormal phenotype of vascular structure and somitogenesis, however, the co-injection with human mutant *RAPGEF1* mRNA did not rescue the phenotype (Figure 6 (C) and (D)).

Discussion:

GTPase-coupled signaling pathways play crucial roles on a multitude of biological functioning scenarios. Among a constellation of genes involved in this signaling pathway, *RAPGEF1* is a guanine nucleotide ex-

change factor responsible for transmitting extracellular signals to the Ras family of GTPase located at the inside of membrane. Mouse modeling unveiled part of the essential roles of *RAPGEF1* in embryonic development, especially that of brain and vessels. However, the involvement of *RAPGEF1* in human Mendelian disease has not yet been identified, although it is intuitive to suppose that the defect of*RAPGEF1* should lead to human disease. Here we report for the first time a case in which two patients with intellectual disability were found to harbor a homozygous mutation of *RAPGEF1* . The correlation of this gene and its mutation with the phenotype was substantiated by genetic analysis and a series of *in silico*prediction. Furthermore, we established a zebrafish model to mimic the symptoms of patients. To the best of our knowledge, this is the first reported zebrafish model for *RAPGEF1* . We confirmed the defective*rapgef1a* , a homologous gene of zebrafish, caused decreased survival rate and abnormal gross morphology including brain pattern and body axis. This model showed significant reduction in movement performance, and an irregular outgrowth of motor neuron axon. Simultaneously, the knockdown of *rapgef1a* led to observable problems in vascular structure and somitogenesis. As a proof-of-concept that the human variant is pathogenic, human wildtype *RAPGEF1* mRNA could largely rescue the abnormal phenotype while the mRNA with the human mutation could not. This finding confirmed the deleterious effect of the human mutation of *RAPGEF1* . To delve into the underlying molecular mechanism of *RAPGEF1* , the zebrafish model that we constructed would be a very good tool, especially in the fields of nervous system and blood vessel development (Covassin et al., 2006; Siekmann & Lawson, 2007).

Acknowledgement:

We are very grateful to the family participating in this study. This work was supported by the Major Medical Collaboration and Innovation Program of Guangzhou Science Technology and Innovation Commission (201604020020), the National Natural Science Foundation of China (81671067, 81974163, and 81701451), the China Postdoctoral Science Foundation (2019M662852), the Natural Science Foundation of Guangdong Province of China (2018A030313538), the Key-Area Research and Development Program of Guangdong Province (2019B020227001) and the German Research Foundation (DFG, SFB1315, FOR3004).

Competing interests:

The authors declare no competing interests.

Data Availability Statement:

Data available on request from the authors.

Author contribution:

H.H. conceived and coordinated the project. T.A.M., A.A.A. and A.M.K. recruited the cohort. N.L., P.Z., and M.M.Y. performed the zebrafish modeling. N.L. was in charge of the genetic analysis and bioinformatics with aids of N.K., X.F.. N.L., A.M.K. and H.H. wrote the manuscript with comments from all authors.

Ethical Statement:

The study was approved by the institutional ethical review boards of Mirpur University of Science and technology (MUST) and by the ethic committee of the Charité (EA1/212/08). Written informed consents were obtained from all individuals or custodians for the participation in the study.

References:

Benedito, R., Rocha, S. F., Woeste, M., Zamykal, M., Radtke, F., Casanovas, O., . . . Adams, R. H. (2012). Notch-dependent VEGFR3 upregulation allows angiogenesis without VEGF-VEGFR2 signalling.*Nature, 484* (7392), 110-114. doi:10.1038/nature10908

Covassin, L. D., Villefranc, J. A., Kacergis, M. C., Weinstein, B. M., & Lawson, N. D. (2006). Distinct genetic interactions between multiple Vegf receptors are required for development of different blood vessel types in zebrafish. *Proc Natl Acad Sci U S A, 103* (17), 6554-6559. doi:10.1073/pnas.0506886103

Hirata, T., Nagai, H., Koizumi, K., Okino, K., Harada, A., Onda, M., . . . Emi, M. (2004). Amplification, up-regulation and over-expression of C3G (CRK SH3 domain-binding guanine nucleotide-releasing factor) in non-small cell lung cancers. *J Hum Genet, 49* (6), 290-295. doi:10.1007/s10038-004-0148-1

Hu, H., Wienker, T. F., Musante, L., Kalscheuer, V. M., Kahrizi, K., Najmabadi, H., & Ropers, H. H. (2014). Integrated sequence analysis pipeline provides one-stop solution for identifying disease-causing mutations. *Hum Mutat, 35* (12), 1427-1435. doi:10.1002/humu.22695

Humphrey, W., Dalke, A., & Schulten, K. (1996). VMD: visual molecular dynamics. *J Mol Graph, 14* (1), 33-38, 27-38. doi:10.1016/0263-7855(96)00018-5

Kanungo, J., Lantz, S., & Paule, M. G. (2011). In vivo imaging and quantitative analysis of changes in axon length using transgenic zebrafish embryos. *Neurotoxicol Teratol, 33* (6), 618-623. doi:10.1016/j.ntt.2011.08.013

Kimmel, C. B., Ballard, W. W., Kimmel, S. R., Ullmann, B., & Schilling, T. F. (1995). Stages of embryonic development of the zebrafish.*Dev Dyn, 203* (3), 253-310. doi:10.1002/aja.1002030302

Kohler, S., Carmody, L., Vasilevsky, N., Jacobsen, J. O. B., Danis, D., Gourdine, J. P., . . . Robinson, P. N. (2019). Expansion of the Human Phenotype Ontology (HPO) knowledge base and resources. *Nucleic Acids Res, 47* (D1), D1018-D1027. doi:10.1093/nar/gky1105

Lawson, N. D., & Weinstein, B. M. (2002). In vivo imaging of embryonic vascular development using transgenic zebrafish. *Dev Biol, 248* (2), 307-318. doi:10.1006/dbio.2002.0711

Martin-Granado, V., Ortiz-Rivero, S., Carmona, R., Gutierrez-Herrero, S., Barrera, M., San-Segundo, L., . . . Guerrero, C. (2017). C3G promotes a selective release of angiogenic factors from activated mouse platelets to regulate angiogenesis and tumor metastasis.*Oncotarget, 8* (67), 110994-111011. doi:10.18632/oncotarget.22339

Nakano, T., Windrem, M., Zappavigna, V., & Goldman, S. A. (2005). Identification of a conserved 125 base-pair Hb9 enhancer that specifies gene expression to spinal motor neurons. *Dev Biol, 283* (2), 474-485. doi:10.1016/j.ydbio.2005.04.017

Nasevicius, A., & Ekker, S. C. (2000). Effective targeted gene 'knockdown' in zebrafish. *Nat Genet, 26* (2), 216-220. doi:10.1038/79951

Noguera-Troise, I., Daly, C., Papadopoulos, N. J., Coetzee, S., Boland, P., Gale, N. W., . . . Thurston, G. (2006). Blockade of Dll4 inhibits tumour growth by promoting non-productive angiogenesis. *Nature, 444* (7122), 1032-1037. doi:10.1038/nature05355

Ohba, Y., Ikuta, K., Ogura, A., Matsuda, J., Mochizuki, N., Nagashima, K., . . . Matsuda, M. (2001). Requirement for C3G-dependent Rap1 activation for cell adhesion and embryogenesis. *EMBO J, 20* (13), 3333-3341. doi:10.1093/emboj/20.13.3333

Paquet, D., Bhat, R., Sydow, A., Mandelkow, E. M., Berg, S., Hellberg, S., . . . Haass, C. (2009). A zebrafish model of tauopathy allows in vivo imaging of neuronal cell death and drug evaluation. *J Clin Invest, 119* (5), 1382-1395. doi:10.1172/JCI37537

Richards, S., Aziz, N., Bale, S., Bick, D., Das, S., Gastier-Foster, J., . . . Committee, A. L. Q. A. (2015). Standards and guidelines for the interpretation of sequence variants: a joint consensus recommendation of the American College of Medical Genetics and Genomics and the Association for Molecular Pathology. *Genet Med, 17* (5), 405-424. doi:10.1038/gim.2015.30

Ridgway, J., Zhang, G., Wu, Y., Stawicki, S., Liang, W. C., Chanthery, Y., . . . Yan, M. (2006). Inhibition of Dll4 signalling inhibits tumour growth by deregulating angiogenesis. *Nature, 444* (7122), 1083-1087. doi:10.1038/nature05313

Sasi Kumar, K., Ramadhas, A., Nayak, S. C., Kaniyappan, S., Dayma, K., & Radha, V. (2015). C3G (Rap-GEF1), a regulator of actin dynamics promotes survival and myogenic differentiation of mouse mesenchymal cells. *Biochim Biophys Acta, 1853* (10 Pt A), 2629-2639. doi:10.1016/j.bbamcr.2015.06.015

Shah, B., Lutter, D., Bochenek, M. L., Kato, K., Tsytsyura, Y., Glyvuk, N., . . . Puschel, A. W. (2016). C3G/Rapgef1 Is Required in Multipolar Neurons for the Transition to a Bipolar Morphology during Cortical Development. *PLoS One, 11* (4), e0154174. doi:10.1371/journal.pone.0154174

Shannon, P., Markiel, A., Ozier, O., Baliga, N. S., Wang, J. T., Ramage, D., . . . Ideker, T. (2003). Cytoscape: a software environment for integrated models of biomolecular interaction networks. *Genome Res, 13* (11), 2498-2504. doi:10.1101/gr.1239303

Siekmann, A. F., & Lawson, N. D. (2007). Notch signalling limits angiogenic cell behaviour in developing zebrafish arteries.*Nature, 445* (7129), 781-784. doi:10.1038/nature05577

Tanaka, S., Morishita, T., Hashimoto, Y., Hattori, S., Nakamura, S., Shibuya, M., . . . et al. (1994). C3G, a guanine nucleotide-releasing protein expressed ubiquitously, binds to the Src homology 3 domains of CRK and GRB2/ASH proteins. *Proc Natl Acad Sci U S A, 91* (8), 3443-3447. doi:10.1073/pnas.91.8.3443

Thompson, J. D., Gibson, T. J., & Higgins, D. G. (2002). Multiple sequence alignment using ClustalW and ClustalX. *Curr Protoc Bioinformatics, Chapter 2* , Unit 2 3. doi:10.1002/0471250953.bi0203s00

Vissers, L. E., Gilissen, C., & Veltman, J. A. (2016). Genetic studies in intellectual disability and related disorders. *Nat Rev Genet, 17* (1), 9-18. doi:10.1038/nrg3999

Voss, A. K., Britto, J. M., Dixon, M. P., Sheikh, B. N., Collin, C., Tan, S. S., & Thomas, T. (2008). C3G regulates cortical neuron migration, preplate splitting and radial glial cell attachment.*Development, 135* (12), 2139-2149. doi:10.1242/dev.016725

Voss, A. K., Gruss, P., & Thomas, T. (2003). The guanine nucleotide exchange factor C3G is necessary for the formation of focal adhesions and vascular maturation. *Development, 130* (2), 355-367. doi:10.1242/dev.00217

Voss, A. K., Krebs, D. L., & Thomas, T. (2006). C3G regulates the size of the cerebral cortex neural precursor population. *EMBO J, 25* (15), 3652-3663. doi:10.1038/sj.emboj.7601234

Westerfield, M. (2000). *The Zebrafish Book: A Guide for the Laboratory Use of Zebrafish (Danio Rerio)* : University of Oregon Press.

Wythe, J. D., Dang, L. T., Devine, W. P., Boudreau, E., Artap, S. T., He, D., . . . Fish, J. E. (2013). ETS factors regulate Vegf-dependent arterial specification. *Dev Cell, 26* (1), 45-58. doi:10.1016/j.devcel.2013.06.007

Zhao, T., Zondervan-van der Linde, H., Severijnen, L. A., Oostra, B. A., Willemsen, R., & Bonifati, V. (2012). Dopaminergic neuronal loss and dopamine-dependent locomotor defects in Fbxo7-deficient zebrafish.*PLoS One, 7* (11), e48911. doi:10.1371/journal.pone.0048911

Figure legends:

Figure 1: Pedigree, clinical, and variant information. (A) Pedigree with two affected individuals from a second-cousin marriage. (B) Sanger sequencing confirmed the heterozygous and homozygous missense variant c.423G>A (NM_198679.1) in the *RAPGEF1* gene in the father III.4 and the patient IV.2, respectively, that had been identified through whole exome sequencing. (C) Clinical information of the two affected individuals in the format of Human Phenotype Ontology (HPO) (Kohler et al., 2019).

Figure 2: Effects of *RAPGEF1* variants. (A) Pathogenicity prediction and population abundances of *RAPGEF1* variant. (B) Distribution of domains of RAPGEF1 and location of the variant. (C) Multiple alignment of protein sequences in species indicated that the variant altered a conserved amino acid. (D) Three-dimensional structural model of RAPGEF1 and a close-up view of structural superposition of RAPGEF1-WT (white) and RAPGEF1-M141I (orange), which were displayed with transparent new cartoon representation. The Met141 and Ile141 residues were shown with white and orange Licorice representation, respectively. The

change of Gibbs free-energy gap (ddG) and the stability upon mutation were also indicated. (E) Modules of protein-protein interaction network included three KEGG pathways, which linked RAPGEF1 (red) and neurodevelopmental genes (green).

Figure 3: Custom-made morpholino nucleotides for zebrafish*rapgef1* and the performance. (A) The zebrafish *rapgef1a*gene was targeted by two specific morpholino antisense strategies to prevent either the translation of the zebrafish gene (ATG-MO) or proper splicing of exon 2 (E2I2-MO). Primers 1F and 3R interrogated the presence of wildtype transcripts or those in which exon 2 was skipped. (B) RT-PCR of *rapgef1a* transcript from Control-MO and E2I2-MO morpholino-injected embryos 3 days after fertilization. Injection of 1 ng of rapgef1a morpholino altered the splicing between exon 2 and intron 2, as revealed by shift in PCR bands between control (315bp) and morpholino-injected embryos (136bp). ef1a served as a negative control to avoid unspecific effects.

Figure 4: Effects of *rapgef1*-knockdown on gross morphology and survival rate. (A) Bright field images and hb9-EGF fluorescent images showed the gross morphology of Control-MO, E2I2-MO and ATG-MO processed zebrafish embryos at 6 hpf. Blue arrows pointed to the abnormal brain patterns. (B) Bright filed images showed the brain patterns of Control-MO, E2I2-MO and ATG-MO processed zebrafish embryos at 6 hpf. Blue arrows pointed to the abnormal brain patterns. Red and yellow arrows indicated the reduction of interorbital distance of the*rapgef1* knockdown zebrafish embryos. (C) Upper: percentage of embryos with defects at 6-hpf in the groups of Control-MO, E2I2-MO and ATG-MO. Lower: a time-course plot of survival rate in the groups of Control-MO, E2I2-MO and ATG-MO for 5 days. (D) Bright field images and hb9-EGF fluorescent images showed the gross morphology of Control-MO, E2I2-MO, E2I2-MO plus mutant human *RAPGEF1* mRNA (E2I2-MO+ MT*RAPGEF1* mRNA), and E2I2-MO plus wildtype human *RAPGEF1*mRNA (E2I2-MO+ WT *RAPGEF1* mRNA) processed zebrafish embryos at 36 hpf. Blue arrows pointed to the abnormal brain patterns. (E) Bright filed images showed the brain patterns of Control-MO, E2I2-MO, E2I2-MO plus mutant human *RAPGEF1* mRNA (MO+MT *RAPGEF1*) , and E2I2-MO plus wildtype human *RAPGEF1* mRNA (MO+WT *RAPGEF1*) processed zebrafish embryos at 36 hpf. Blue arrows pointed to the abnormal brain patterns. Red and yellow arrows indicated the reduction of interorbital distance of the *rapgef1* knockdown zebrafish embryos. (F) Upper: percentage of embryos with defects at 36-hpf in the groups of Control-MO, E2I2-MO, E2I2-MO plus mutant human *RAPGEF1*mRNA (E2I2-MO+ MT *RAPGEF1* mRNA), and E2I2-MO plus wildtype human*RAPGEF1* mRNA (E2I2-MO+ WT *RAPGEF1* mRNA). Lower: a time-course plot of survival rate in the groups of Control-MO, E2I2-MO, E2I2-MO plus mutant human *RAPGEF1* mRNA (E2I2-MO+ MT*RAPGEF1* mRNA), and E2I2-MO plus wildtype human *RAPGEF1*mRNA (E2I2-MO+ WT *RAPGEF1* mRNA) for 5 days. hpf: hours post fertilization.

Figure 5: Effects of *rapgef1*-knockdown on locomotor capacity and motor neuron development. (A) Digital tracks and heatmap images of zebrafish larvae at 5-dpf in the groups of Control-MO, E2I2-MO, and ATG-MO. (B) Statistical analysis on the four parameters of movement in the three aforementioned groups, namely, total distance, velocity, mobility, and maximal acceleration. * $P < 0.05$, ** $P < 0.01$, $N = 4$, ANOVA. (C) Digital tracks and heatmap images of zebrafish larvae at 5-dpf in the groups of Control-MO, E2I2-MO, E2I2-MO plus mutant human *RAPGEF1* mRNA, and E2I2-MO plus wildtype human*RAPGEF1* mRNA. (D) Statistical analysis on the four parameters of movement in the four aforementioned groups, namely, total distance, velocity, mobility, and maximal acceleration. * $P < 0.05$, ** $P < 0.01$, *** $P < 0.001$, ns: not significant, $N = 6$, ANOVA. (E) Gross morphology of *Tg(hb9:EGFP)* zebrafish embryos at 36-hpf in the groups of Control-MO, E2I2-MO, and ATG-MO. The spinal motor neurons were visualized by EGFP fluorescence. Irregular motor neuron axons were labeled by asterisk. (F) Gross morphology of*Tg(hb9:EGFP)* zebrafish embryos at 48-hpf in the groups of Control-MO, E2I2-MO, E2I2-MO plus mutant human *RAPGEF1* mRNA (E2I2-MO+ MT *RAPGEF1* mRNA), and E2I2-MO plus wildtype human*RAPGEF1* mRNA (E2I2-MO+ WT *RAPGEF1* mRNA). The spinal motor neurons were visualized by EGFP fluorescence. Irregular motor neuron axons were labeled by asterisk. (G) Upper: quantification of the average length of motor neuron axon in the groups of Control-MO, E2I2-MO, and ATG-MO. Lower: quantification of the average length of motor neuron axon in the groups of Control-MO, E2I2-MO, E2I2-MO plus mutant human*RAPGEF1* mRNA (E2I2-MO+ MT *RAPGEF1* mRNA), and E2I2-MO plus wildtype human *RAPGEF1* mRNA (E2I2-MO+

WT *RAPGEF1* mRNA). ** P < 0.01, *** P < 0.001, N = 10, ANOVA. dpf: days post fertilization. hpf: hours post fertilization.

Figure 6: Effects of *rapgef1*-knockdown on vascular development and somitogenesis. (A) Bright field and fluorescent images of *Tg(fli1a:EGFP)* zebrafish embryos at 72-hpf in the groups of Control-MO, E2I2-MO, and ATG-MO. Vascular structure was visualized by EGFP fluorescence. Labels were used for ISV (intersegmental vessel), DLAV (dorsal longitudinal anastomotic vessel), DA (dorsal aorta), PCV (posterior cardinal vein), and sprouts. (B) Gross somite morphology at 3-dpf in the groups of Control-MO, E2I2-MO, and ATG-MO. Dotted lines delineated somite boundaries. (C) Bright field and fluorescent images of zebrafish embryos at 72-hpf in the groups of Control-MO, E2I2-MO, E2I2-MO plus mutant human *RAPGEF1* mRNA (E2I2-MO+ MT*RAPGEF1* mRNA), and E2I2-MO plus wildtype human *RAPGEF1*mRNA (E2I2-MO+ WT *RAPGEF1* mRNA). Vascular structure was visualized by EGFP fluorescence. Labels were used for ISV (intersegmental vessel), DLAV (dorsal longitudinal anastomotic vessel), DA (dorsal aorta), PCV (posterior cardinal vein), and sprouts. (D) Gross somite morphology at 3-dpf in the groups of Control-MO, E2I2-MO, E2I2-MO plus mutant human *RAPGEF1* mRNA (E2I2-MO+ MT *RAPGEF1* mRNA), and E2I2-MO plus wildtype human *RAPGEF1* mRNA (E2I2-MO+ WT*RAPGEF1* mRNA). Dotted lines delineated somite boundaries. dpf: days post fertilization. hpf: hours post fertilization.

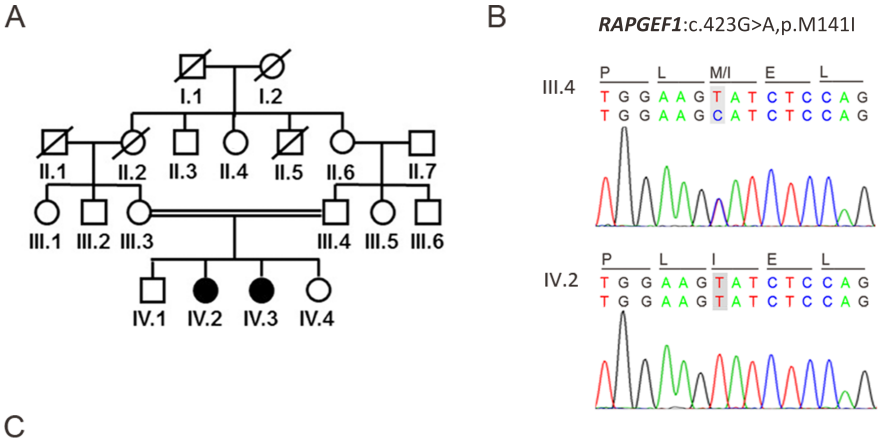

C

Gene	Patient	Gender	OFC[1] [cm]	Height [cm]	Weight [kg]	Age at examination [y]	Phenotype HPO	ID[2] 0001249	Moderate ID 0002342	Speech impairment 0002167	Dull facial expression 0000338	Behavioral abnormality 0000708	Repetitive behavior 0000732	visual impariment 0000505
RAPGEF1	IV.2	female	55.88	155	68	18		+	+	-	+	+	+	+
	IV.3	female	54.6	155	60	16		+	+	+	+	+	+	+

1. OFC: Occipitofrontal circumference; 2. ID: Intellectual disability

A

Gene	Chromosomal Position (GRCh37/hg19)	Transcript	Variant	Inheritance	HGMD	OMIM	dbSNP153	1000Genome	ESP6500	GnomAD	SIFT	PolyPhen2	Mutation-Taster
RAPGEF1	g.9:134518700 C>T	NM_198679	c.423G>A, p.M141I	Autosomal recessive	-	-	-	-	-	-	deleterious	possibly damaging	disease causing